IOP Publishing Journal of Physics: Condensed Matter
J. Phys.: Condens. Matter **32** (2020) 165701 (9pp) https://doi.org/10.1088/1361-648X/ab6710

T-C_{56}: a low-density transparent superhard carbon allotrope assembled from C_{16} cage-like cluster

Yanqing Guo[1], Leyuan Cui[1], Ding Zhao, Tielei Song, Xin Cui and Zhifeng Liu[2]

School of Physical Science and Technology, Inner Mongolia University, Hohhot 010021, People's Republic of China

E-mail: zfliu@imu.edu.cn

Received 4 November 2019, revised 30 November 2019
Accepted for publication 2 January 2020
Published 23 January 2020

Abstract

Owing to the various ways of chemical bonding, carbon can form abundant allotropes with different frameworks, which harbor rich mechanical and electronic properties. Taking the cage-like isomer of C_{16} cluster as a building block, we design a new low-density carbon allotrope, which has tetragonal symmetry (*I*4/*mmm*) and a 56-atom unit cell, hence termed as T-C_{56}. Our first-principles calculations reveal that T-C_{56} is not only energetically, dynamically, thermally (above 1800 K) and mechanically stable, but even more stable than the experimentally synthesized C20-sc and T-carbon. Remarkably, although the framework of T-C_{56} is low density (2.72 g cm^{-3}), it exhibits novel superhard properties with a Vickers hardness of 48.71 GPa. The obtained Yang's modulus and ideal strength show that T-C_{56} is mechanically anisotropic. In particular, our analysis of electronic and optical properties suggest that T-C_{56} is a transparent indirect semiconductor with a wide bandgap of 3.18 eV (HSE06). These findings highlight a distinct carbon allotrope, having promising applications for optical and aerospace devices due to its light, transparent, superhard features.

Keywords: carbon allotrope, light superhard material, first-principles calculations, mechanical anisotropy, electronic and optical properties

(Some figures may appear in colour only in the online journal)

1. Introduction

As a common element, carbon is widely distributed in the atmosphere, lithosphere and organism. In a special position of element periodic table, carbon has four outermost electrons $2s^2 2p^2$ outside the nucleus; thus can forms various chemical bonds including *sp*, sp^2 and sp^3 hybrid modes. Because of such particular feature, a lot of carbon allotropes with different dimensions (e.g. 0D fullerene [1], 1D nanotube [2], 2D graphene [3] and 3D diamond) [4] have been experimentally identified. Carbon has become a typical system to demonstrate the fact that different bonding modes lead to diverse atomic structures, and then result in versatile properties. Taking 3D carbon allotropes as examples, the layered graphite with sp^2-hybrid mode exhibits metallicity due to freely moving electrons [5] the graphene networks, such as MTC [6] (all-sp^2) and IGN [7] hold topological semimetallicity; the Bct C_8 regarded as the compressure of carbon nanotubes with sp^3 hybridization is a semiconductor [8]; the I-43d carbon structure with sp^3 hybridization in tetrahedral networks is confirmed as the carbon allotrope with the largest band gap [9]. Additionally, many 3D carbon allotropes constructed by sp^3-bonded atoms have been proved to be superhard materials because of large C-C binding energy, such as C_{20}-T [10], S-carbon [11], H-carbon [11], M_{585} [12], Z-ACA [13], C21-sc [14], clathrate-like 215-10-III-4-001 [15], M carbon [16], W carbon [17], Cco-C_8 [18], and so on. In this context, more and more efforts

[1] Equal contribution to this work.
[2] Author to whom any correspondence should be addressed.

have been devoted to propose or synthesize new carbon materials [9–34], which are expected to be the foundation of the future carbon-based electronics [35–37].

Under extreme physic conditions, the superhard materials are essential for industrial applications (e.g. cutting tools, special wear-resistant parts, aerospace and cosmic devices) due to their incompressibility and wear-resistance. On the basis of mass density ρ, the reported superhard carbon allotropes can be classified into two categories: high and low density superhard materials, whose $\rho > 3$ g cm^{-3} and $\leqslant 3$ g cm^{-3}, respectively. Generally, the high density superhard carbon allotropes can be obtained by high-pressure processing [16–21]. For instance, when graphite is cold-compressed above 13.4 GPa, a more stable carbon allotrope, M-carbon ($\rho = 3.34$ g cm^{-3} and $H_v = 83.1$ GPa) [16], has been identified by *ab initio* calculations; under a constant pressure of 15 GPa, the *Cmmm* symmetric Z-carbon [19] was found by the minima hopping search method, whose density and Vickers hardness are 3.40 g cm^{-3} and 95.4 GPa, respectively; by compression of a (10, 10) carbon nanotube lattice to 20 GPa, a intriguing polymorph, bct-C_4 [20], was characterized as a superhard material with Vickers hardness of 88 GPa, whose mass density is 3.31 g cm^{-3}. Interestingly, some low-density carbon phases [38–40] have also been confirmed as superhard materials due to the strong sp^3 C–C bonds, such as Hex-C_{18} ($\rho = 2.41$ g cm^{-3} and $H_v = 42.2$ GPa) [38] and Hex-C_{24} ($\rho = 2.75$ g cm^{-3} and $H_v = 44.54$ GPa) [39]. However, compared with the high-density superhard allotropes, the light weight low-density superhard phases are quite rare. As a matter of fact, the light superhard materials are quite necessary for the aerospace applications. Hence, it is very significant to find or design a new low-density superhard carbon allotrope, which may further extend the range of properties and applications of carbon-based materials.

Since the discovery of C_{60} fullerene [41], the carbon cages constructed solids have attracted numerous attentions from researchers in both experiment and theory fields [42–51]. In experiment, the C_{70} cage polymerized solid [48] has been synthesized under 2 gigapascals hydrostatic pressure; the C_{36}-cage assembled crystal has been produced through the arc-discharge method [49]. In theory, using first-principles calculation the C_{96} carbon [50] has been identified as a hollow nanotube network built from the C_{24} and C_{18} cages; the C_{60} clathrate [51] constructed by small C_{24} and flat C_{18} cages was proposed as a superhard superstrong open framework. Inspired by these works, we identified a distinct low-density superhard carbon allotrope by taking the stable cage isomer of C_{16} cluster [52] composed of two C_4 rings and eight C_5 rings as the building blocks. From the first-principles calculations, we confirmed that this new phase is tetragonal symmetry (*I*4/*mmm*) with 56 atoms in each unit cell, named T-C_{56}. Based on the calculations of elastic constants, the obtained Vickers hardness of T-C_{56} is 48.71 GPa, larger than the hardness criterion (40 GPa) of superhard materials [53], implying that T-C_{56} is a typical superhard material. Our HSE06 calculations of electronic band structure and density-of-states show that T-C_{56} is a optical transparent semiconductor with an indirect bandgap about 3.18 eV. The stabilities of T-C_{56} have been systematically investigated by examining the total energy, elastic constants, phonon spectrum, and the first-principles molecular simulation.

2. Computational details

Our first-principles calculations were carried out using the Vienna *ab initio* simulation program package (VASP) [54]. The exchange-correlation effects were described by the Perdew–Burke–Ernzerhof (PBE) function of generalized gradient approximation [55]. During the structural optimizations, the convergence criterions of atomic forces and total energy were set as 10^{-2} eV Å^{-1} and 10^{-6} eV, respectively. The tested cutoff energy of 520 eV was adopted for the plane-wave expansion of valence electrons so as to ensure that the total energies converge to 0.001 eV per atom. Brillouin zone integration was performed for $\boldsymbol{k}$-point meshes generated by the Gamma scheme with a grid density of $2\pi \times 0.03$ Å^{-1}. The elastic constants were calculated from the evaluation of stress tensor generated small strain; the bulk modulus, shear modulus and Young's modulus were derived from the Voigt–Reuss–Hill approximation [56]. Meanwhile the Vickers hardness of T-C_{56} was estimated by the Chen *et al* model [57]. Phonon mode calculation was performed using PHONOPY package [58] with the forces calculated from VASP.

3. Results and discussion

3.1. Structural properties

In the C_{16} cage cluster (C_{4v} point group), there are two opposite C_4 rings with a rotational angle of 45°, both of which connect four C_5 rings [52]. On the basis of these structural features, we consider three types of cluster-cluster links, i.e. coplane (CP), square (S) and line (L) links, as illustrated in figure 1(a). If every C_{16} cage is connected by nine C_{16} clusters (i.e. four S-linked, four L-linked and one CP-linked clusters, see figure 1(b)), a 3D solid structure can be obtained through periodic translations of the central cage. During this built processing, two additional kinds of carbon cages (C_{20} [$4^4 5^4 6^4$] and C_{40} [$4^2 5^8 6^{12}$]) can be formed, as displayed in figure 1(c). Notably, the C_{4v} symmetric geometry of C_{16} cage is well preserved in the optimized solid structure (see figure 1(d)). Its unit cell exhibits tetragonal symmetry and has 56 carbon atoms. Hence, we call it as T-C_{56}. Four inequivalent atoms occupying the Wyckoff position 8*j* (0.5, 0.2947, 0.0), 16*n* (0.5, 0.1593, 0.1043), 16*m* (0.7208, 0.2792, 0.1635) and 16*m* (0.8692, 0.1308, 0.2328) can be found in every unit cell. The related structure parameters of T-C_{56} and some considered allotropes are listed in table 1. For T-C_{56}, the optimized lattice constants of *a* and c are 5.60 Å and 13.07 Å, respectively. Owing to the existence of hollow cages, especial the C_{40} [$4^2 5^8 6^{12}$] cages, the mass density of T-C_{56} (2.72 g cm^{-3}) is smaller than that of diamond (3.50 g cm^{-3}). Therefore, T-C_{56} is a typical low-density carbon allotrope according to the mentioned criterion of 3 g cm^{-3}.

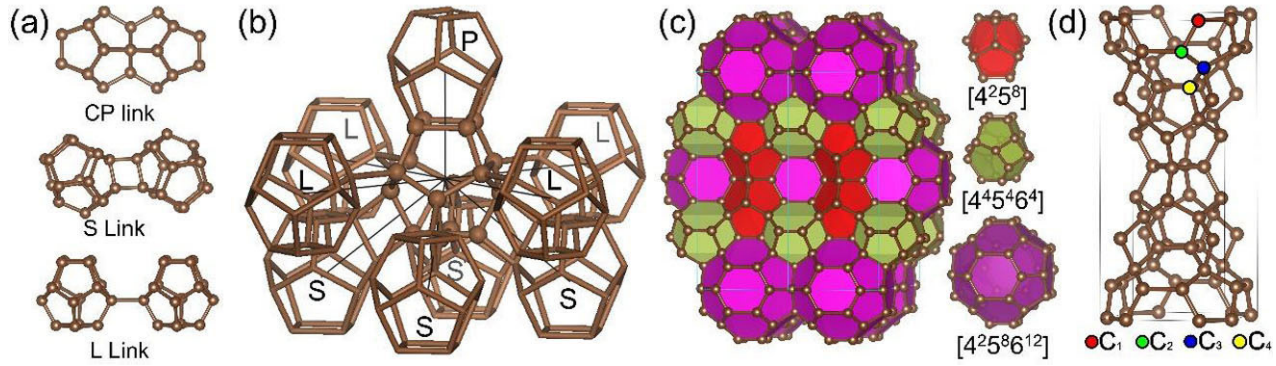

Figure 1. (a) Three kinds of links between C_{16} clusters. (b) Coordination of every C_{16} cage in the T-C_{56}. (c) The illustration of T-C_{56} crystal structure with three types of colorized cage-like polyhedrons, i.e. C_{16} [$4^2 5^8$], C_{20} [$4^4 5^4 6^4$] and C_{40} [$4^2 5^8 6^{12}$]. (d) The unit cell of T-C_{56} phase with four kinds of inequivalent carbon atoms C_1, C_2, C_3 and C_4.

Table 1. The calculated space group (SG), lattice constant (a, c), total energy (E_{tot}), equilibrium density (ρ), energy gap (E_g),volume (V) for diamond, Hex-C_{24}, C_{64}, C_{20}-T, C20-sc, T-carbon, and T-C_{56}.

Structure		*SG*	*a*,*c*	*V*	ρ	E_{tol}	E_g
Diamond	Our	*Fd*-3*m*	3.57	5.70	3.50	−9.09	4.02
	Exp [59]		3.57	5.67	3.51		
	Exp [60]			5.67			5.47
Hex-C_{24}	Our	*P*63/*mcm*	6.90, 4.22	7.25	2.75	−8.96	—
	Bu *et al* [39]		6.83, 4.17		2.84	−8.07	—
C_{64}	Our	*I*41/*amd*	7.18, 9.67	7.79	2.56	−8.81	1.30
	Wei *et al* [40]		7.18, 9.66	7.79	2.56		
C_{20}-T	Our	P213	4.95	6.06	3.29	−8.50	4.13
	Wang *et al* [10]		4.95		3.30	−8.50	
C20-sc	Our	Pm-3m	5.22	7.10	2.81	−8.47	—
	He *et al* [14]		5.16		2.89	−8.32	—
T-carbon	Our	*Fd*-3*m*	7.52	13.27	1.50	−7.92	2.17
	Exp [25]		7.52		1.50	−7.463	2.25
T-C_{56}	PBE	*I*4/*mmm*	5.60, 13.07	7.33	2.72	−8.56	2.26
	HSE06						3.18

3.2. Stabilities

Is the porous low-density T-C_{56} phase stable? To examine the energy stability of T-C_{56}, we computed the total energy per atom as a function of the volume. For comparison, six related carbon allotropes including diamond, Hex-C_{24}, C_{64}, C_{20}-T, and the synthesized T-carbon and C20-sc have also been considered, as shown in figure 2(a). Generally, the phase with lower equilibrium energy should be more stable. By fitting the third-order Birch–Murnaghan equations of state [61]:

$$E_t(V) = E_0 + \frac{9}{16} B_0 V_0 \left[(B' - 4) \left(\frac{V_0}{V} \right)^{\frac{2}{3}} - B' + 6 \right] \left[\left(\frac{V_0}{V} \right)^{\frac{2}{3}} - 1 \right]^2, \quad (1)$$

we confirmed that the energetic ordering of these considered phases is $E_{diamond} < E_{Hex\text{-}C24} < E_{C64} < E_{T\text{-}C56} < E_{C20\text{-}T} < E_{C20\text{-}sc} < E_{T\text{-}carbon}$. Although the equilibrium total energy of T-C_{56} (−8.56 eV/atom) is higher than that of diamond (−9.09 eV/atom), Hex-C_{24} (−8.96 eV/atom) and C_{64} (−8.81 eV/atom), it is energetically more favorable than the experimentally synthesized C20-sc [14] and T-carbon [22]. This can be understood by the fact that the average bond angle (108.88°) of T-C_{56} is closer to the perfect bond angle (109.47°) of tetrahedral coordinate sp^3 hybridization than that of T-carbon (102.37°) and sp^2–sp^3 hybridezed carbon allotrope C20-sc (114.52°). Additionally, to confirm the stability of T-C_{56} with respect to the synthesized phases (e.g. diamond, C20-sc and T-carbon) in different ranges of pressures, we further derived their enthalpies $H(P)$ at 0–100 GPa from the Birch–Murnaghan fitted EOS plots in figure 2(a) by:

$$H = E_t + PV, \quad (2)$$

where the pressure P and volume V obey the following equation:

$$P = \frac{3}{2} B_0 \left[-\left(\frac{V_0}{V} \right)^{\frac{5}{3}} + \left(\frac{V_0}{V} \right)^{\frac{7}{3}} \right] \left[1 + \frac{3}{4} (B_1 - 4) \left(\frac{V_0}{V} \right)^{\frac{2}{3}} \right]. \quad (3)$$

At a given pressure, a more stable phase usually has a lower enthalpy. As displayed in figure 2(b), one can find that T-C_{56} is more stable than the synthesized C20-sc and T-carbon in the whole considered pressures of 0–100 GPa.

To check the dynamic stability of T-C_{56}, we computed the phonon spectrum of T-C_{56} in the entire Brillouin zone. As illustrated in figure 2(c), no imaginary frequencies can

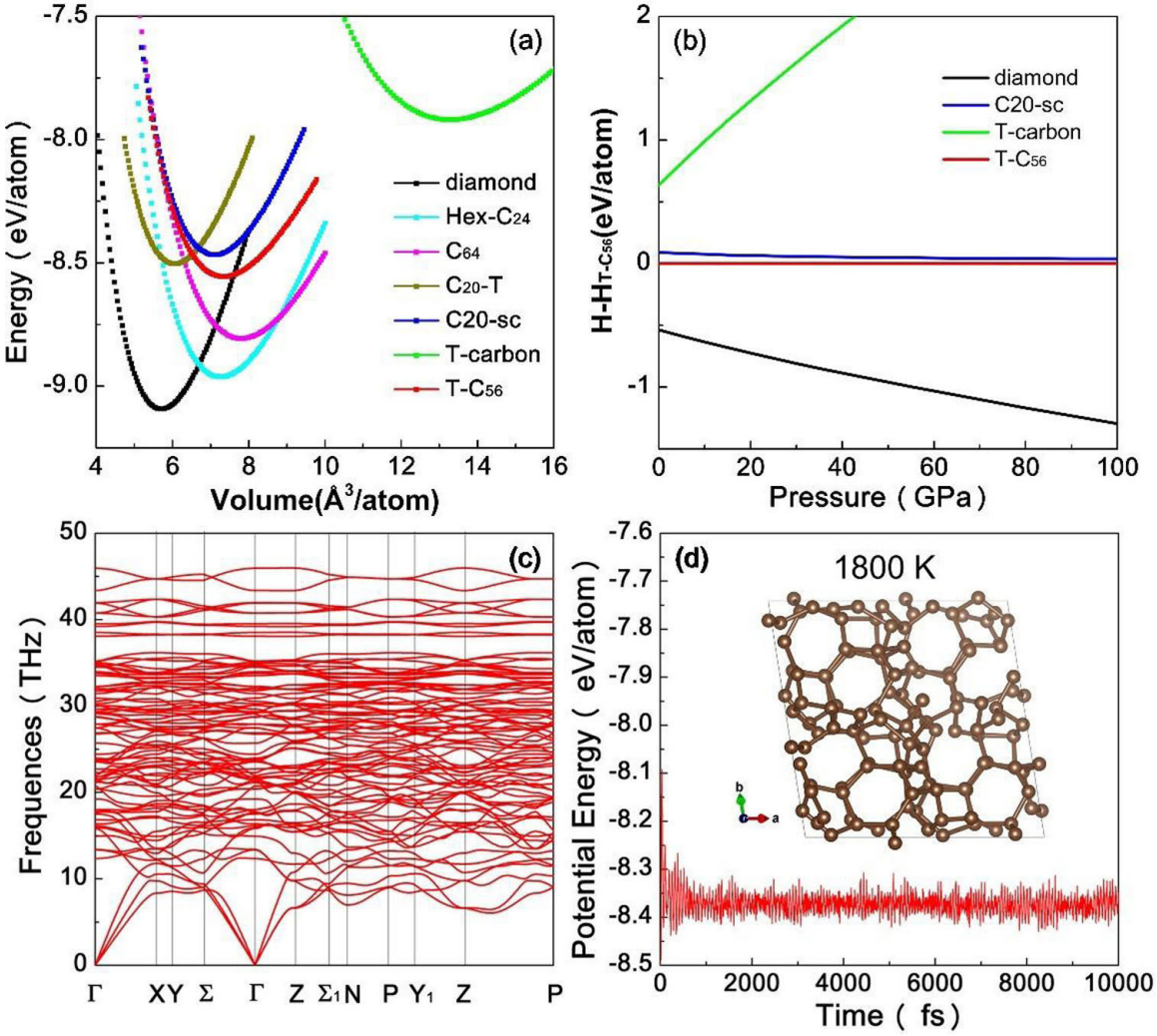

Figure 2. (a) The total energy as a function of volume per atom for T-C_{56} clathrate, together with diamond, Hex-C_{24}, C_{64}, C_{20}-T, C20-sc and T-carbon. (b) The enthalpies H per atom as a function of pressure for the considered carbon allotropes (diamond, C20-sc and T-carbon) with respect to T-C_{56}. (c) Phonon band structure and (d) potential energy fluctuation during 10 000 fs FPMD simulations for T-C_{56}. The inset is the snapshot of the supercell of T-C_{56} at the end of simulation.

be seen, demonstrating that T-C_{56} is dynamically stable at $T = 0$ K. However, this can not ensure that the T-C_{56} phase will not be destroyed at elevated temperatures, especially when its structure corresponds to a shallow minimum on the potential energy surface. Therefore, it is necessary to further explore the thermal stability of the dynamically stable T-C_{56}. By building a $2 \times 2 \times 1$ supercell with 112 atoms, we performed the first-principles molecular dynamics (FPMD) simulations at 1000 K, 1500 K and 1800 K with Nose-Hoover thermostat. During the 10 ps simulation times, the potential energies of T-C_{56} almost keep a constant with small variations coursed by the thermal fluctuations at all of the considered temperatures. Figure 2(d) presents the potential energy fluctuation as a function of simulation times at 1800 K. The constant potential energies indicate that there is no geometry reconstruction in T-C_{56} at the 1800 K. Therefore, we can conclude that our proposed T-C_{56} can withstand temperatures as high as 1800 K. Namely, the structure of T-C_{56} is separated by high-energy barriers from other local minima on the corresponding potential energy surface.

Moreover, one may also wonder whether the T-C_{56} is mechanically stable. For a stable tetragonal crystal phase, the six independent elastic constants (i.e. C_{11}, C_{33}, C_{44}, C_{66}, C_{12} and C_{13}) should simultaneously obey the Born mechanical stability criteria [65]: $C_{11} > 0$, $C_{33} > 0$, $C_{44} > 0$, $C_{66} > 0$, $(C_{11} - C_{12}) > 0$, $(C_{11} + C_{33} - 2C_{13}) > 0$ and $[2(C_{11} + C_{12}) + C_{33} + 4C_{13}] > 0$. Using strain-stress relationship [66], the C_{11}, C_{33}, C_{44}, C_{66}, C_{12} and C_{13} of T-C_{56} are calculated to be 520, 784, 296, 244 and 109 GPa (see table 2), respectively. Obviously, they meet all the mentioned criteria, indicating that T-C_{56} is mechanically stable.

3.3. Electronic and optical properties

The electronic band structure of T-C_{56} along the high-symmetry ***k***-points is shown in figure 3(a). The valence band maximum locates at the special point X, while the conduction band minimum appears at Z. In this regard, T-C_{56} is a typical indirect semiconductor. However, the estimated indirect bandgap (2.26 eV) is very close to the direct bandgap at

Table 2. Calculated elastic constants (C_{ij}, GPa), bulk modulus (B, GPa), shear modulus (G, GPa), Yang's modulus (Y, GPa), B/G, Poisson's ratio (ν) and Vickers hardness (H_v, GPa) of T-C_{56}, along with that of diamond, Hex-C_{24}, C_{64}, C_{20}-T, C20-sc and T-carbon at zero pressure. For comparison, the reported data are also presented.

Structure		C_{11}	C_{33}	C_{44}	C_{66}	C_{12}	C_{13}	B	G	B/G	ν	H_v
Diamond		1074		571		139		451	527	0.86	0.08	90.95
	[a]	1106		607		141		462	545		0.08	
	[b]	1076		577		125		442				91.76
Hex-C_{24}		595	1069	331		183	193	365	279	1.31	0.20	36.26
	[c]	609	1102	325		189	83					44.54
C_{64}			578	684	245	106	42	117	328	316	1.04	0.14
	[d]	598	677	254	107	43	108					33.92
C_{20}-T		956		375		98		384	396	0.97	0.12	65.52
	[e]	994		412		95		395	427	0.93	0.11	72.76
C20-sc		512		240		241		331	191	1.74	0.26	19.64
	[f]	577		244		276		370	196			91.44
T-carbon		190		67		140		156	45	3.47	0.36	1.33
	[g]							169	70			5.6
T-C_{56}		519	784	296	244	109	99	267	265	1.01	0.13	48.77

[a] Fan *et al* [62].
[b] Exp [63].
[c] Bu *et al* [39].
[d] Wei *et al* [40].
[e] Wang *et al* [10].
[f] He *et al* [14].
[g] Chen *et al* [64].

X point (2.33 eV), thus T-C_{56} should be a quasi-direct semiconductor, like the reported C_{64} [40]. As is well known, the bandgap of semiconductor will be significantly underestimated by the PBE method. Herein, we adopted the state-of-the-art hybrid functional (HSE06) [67] to recalculate the band structure of T-C_{56}. As presented in figure 3(a), the bands from HSE06 are similar to that of PBE, but the position of conduction bands is significantly up-shifted and that of valence bands is down-shifted. This results in a larger indirect bandgap (3.18 eV) and direct bandgap (3.29 eV), which should be more accurate and consistent with the future experimental value. To obtain a deeper understanding for the electronic properties of T-C_{56}, we calculated the projected density of states on the four inequivalent carbon atoms (figure 3(b)) and different atomic orbitals (figure 3(c)). From the figures, we can clearly see that the valence band edge states are dominated by C_1 atoms and $p_x + p_y$ orbitals, while the conduction band edge states mainly come from C_4 atoms and $s + p_z$ orbitals. Owing to the wide bandgap which is larger than the energies of the visible light, the proposed T-C_{56} should be an optical transparent material. To confirm this fact, we further calculate the imaginary part of the dielectric function of T-C_{56} from both PBE and HSE06 methods (see figure 3(d)). The optical adsorption starts at the direct gap transition energy 3.29 eV (HSE06), indicating that the direct gap transition in T-C_{56} is dipole allowed. The peak of the optical adsorption locates at the deep ultraviolet region (9.96 eV). Obviously, there is no adsorption in the visible region (1.61 eV–3.10 eV) at all. So T-C_{56} is an optical transparent material.

3.4. Mechanical properties

As discussed above, T-C_{56} is a low-density porous carbon allotrope. Naturally, one may ask whether it can preserve its intrinsic configuration under extremely mechanical condition? To assess the mechanical resistance to external forces in different ways, we firstly calculated the bulk modulus (B, the average of B_v and B_R) and shear modulus (G, the average of G_V and G_R) of T-C_{56} by the Voigt–Reuss–Hill approximation [56]. On the basis of the obtained elastic constants, the B_v, B_R, G_V and G_R are respectively obtained by the following equations:

$$B_V = \frac{1}{9}[2(C_{11} + C_{22}) + C_{33} + 4C_{13}], \tag{4}$$

$$B_R = \frac{(C_{11} + C_{12})C_{33} - 2C_{13}^2}{C_{11} + C_{12} + 2C_{33} - 4C_{13}}, \tag{5}$$

$$G_V = \frac{1}{15}(C_{33} - 2C_{13} + 2C_{11} - C_{12} + 6C_{44} + 3C_{66}), \tag{6}$$

and

$$G_R = 15\left\{\frac{18B_V}{(C_{11} + C_{12})C_{33} - 2C_{13}^2} + [6(C_{11} - C_{12})] + \frac{6}{C_{44}} + \frac{3}{C_{66}}\right\}. \tag{7}$$

The obtained results are listed in table 2. Overall, bulk modulus and shear modulus of T-C_{56} are smaller than the corresponding value of diamond, but larger than that of synthesized T-carbon [22]. Specifically, the bulk modulus of T-C_{56} is 267 GPa, 59% of that of diamond. However, it is greatly larger

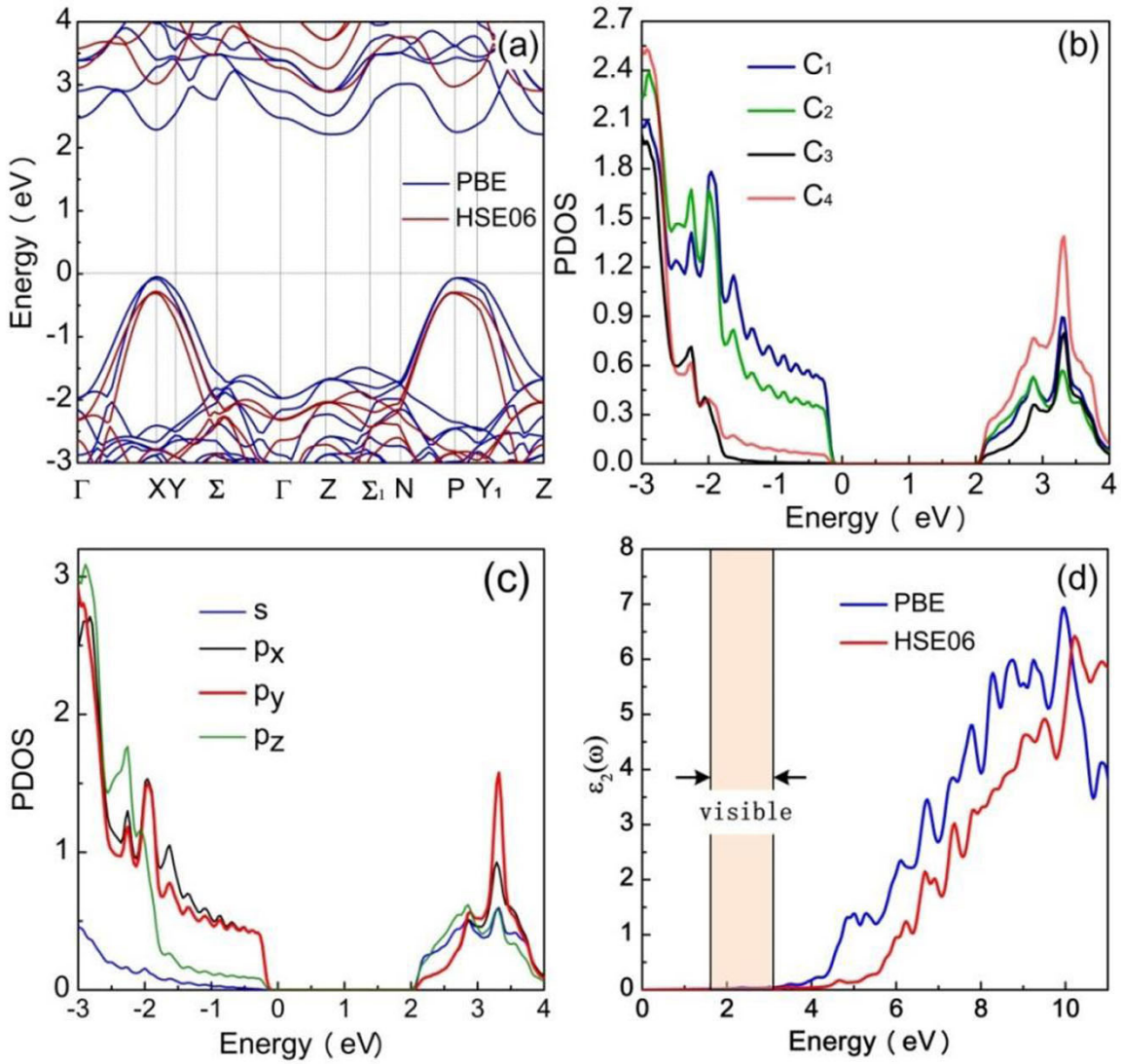

Figure 3. (a) The electronic band structures of T-C_{56} calculated in PBE (see the blue lines) and HSE06 (see the red lines) theory levels. The corresponding projected density of states (b) on the four inequivalent carbon atoms and (c) on the different atomic orbitals of T-C_{56}. (d) Imaginary part of dielectric function as a function of energy for T-C_{56} computed from the PBE and HSE06 methods.

(1.71 times) than that of T-carbon. Moreover, the *B*/*G* ratio is used to characterize the brittle or ductile behavior of a material. High (low) *B*/*G* ratio is often corresponding to ductility (brittleness) with the critical value of 1.75 proposed by Paugh [68]. For T-C_{56}, the calculated *B*/*G* ratio is 1.01, which is lower than the critical value, suggesting that its structure is brittle. Since it is smaller than that of T-carbon (3.47), it is more ductile with respect to T-carbon. Moreover, the brittleness/ductility of a material can also be examined by the Frantsevich rule adopting the Poisson's ratio [69]. Usually, a high (low) Poisson's ratio is associated with ductility (brittleness) with the critical ratio of 1/3. The Poisson's ratio of T-C_{56} is calculated to be 0.13, smaller than that (0.36) of T-carbon, implying that it is brittle. This is consistent well with the result from the *B*/*G* ratio.

To examine the mechanical anisotropy of T-C_{56}, we further calculated the direction-dependent Young's modulus by the following equation [70]:

$$Y = \frac{1}{S_{11}(l_1^4 + l_1^4) + S_{33}l_3^4 + (S_{44} + 2S_{13})(l_1^2 + l_2^2)l_3^2 + (S_{66} + 2S_{12})(l_1 \times l_2)^2}, \tag{8}$$

where S_{ij} is the inverse of elastic constant matrix C_{ij}, $l_1 = \sin\theta\cos\varphi$, $l_2 = \sin\theta\sin\varphi$, $l_3 = \cos\theta$ refer to the directional parameters to three principal axes. Figure 4(a) plots the surface contours of Young's moduli of T-C_{56} in different directions. From the whole 3D shape and the color bar, one can see that the Young's moduli of T-C_{56} exhibit anisotropy with a sizable ratio of 1.54 between the maximum value (753 GPa) and maximum value (489 GPa). Specifically, the Young's modulus along *x* axis is equal to that in *y* axis due to the tetragonal symmetry, which holds the minimum (see figure 4(b)). Along the [1 1 0] direction, the Young's modulus reaches its maximal value of 540 GPa. In the (1 0 0) plane (figure 4(c)), one can find that the maximum of Young's modulus is in the [0 0 1] direction, while the minimum is in the [1 0 0] orientation.

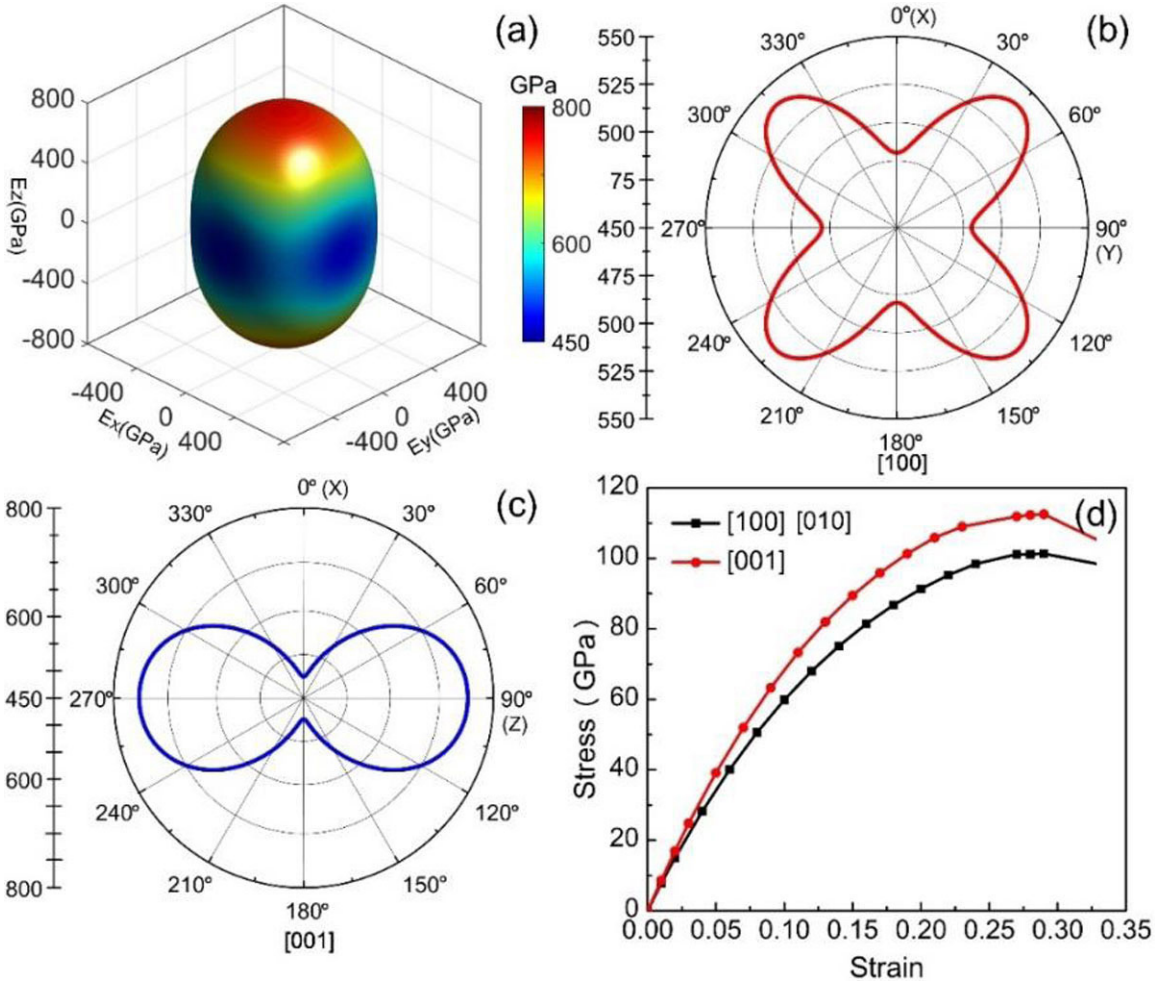

Figure 4. (a) Surface contours of Young's moduli of T-C_{56} in different directions. (b) The projected Young's moduli (b) on the (0 0 1) plane and (c) on the (1 0 0) plane. (d) The calculated ideal tensile strengths of T-C_{56} along [1 0 0], [0 1 0] and [0 0 1] directions.

To provide another perspective for the mechanical anisotropy, we computed the tensile strength along some typically crystal directions, including the three principles axes [1 0 0], [0 1 0] and [0 0 1]. The mechanical stresses as a function of the applied external strain are presented in figure 4(d). From this figure, we can also conclude that T-C_{56} is mechanically anisotropic. In details, one can find two specific conclusions: (i) owing to the tetragonal symmetry, the ideal strengths (101 GPa) in [1 0 0] and [0 1 0] axes are equal, which is larger than the ideal tensile strength of 71.1 GPa along [1 1 0] for C_{20}-T [10]; (ii) in the [0 0 1] axis, the ideal strength possesses a larger value (131 GPa). These results are consisting with our analysis of Young's modulus.

To further characterize the mechanical strength of T-C_{56}, we calculated its Vickers hardness [71], which is defined as an ability to resist the external deformations, such as denting, scratching, or bending. Here, the H_v of T-C_{56} was calculated by the empirical formula proposed by Chen *et al* [57]:

$$H_v = 2(k^2G)^{0.585} - 3 \quad (9)$$

which usually gives better results for anisotropic materials, and has been widely used for identifying the candidate superhard materials [72–74]. In the formula, the k is the Pugh's modulus ratio defined as the ratio of shear modulus G to bulk modulus B. For our predicted T-C_{56}, its Vickers hardness is computed to be 48.71 GPa. Moreover, for comparison we have also calculated the Vickers hardness of some other allotropes (see H_v in table 2). Although the value is only about a half of the hardness of diamond (90.75 GPa), it is greatly larger than that of T-carbon (1.3 GPa), Hex-C_{24} (36.26 GPa), C_{64} (32.13 GPa) and C20-sc (17.79 GPa). More importantly, it is larger than the critical value of 40 GPa, which is a recognized criterion for identifying the candidates of superhard materials [53]. Therefore, T-C_{56} should be a particular low-density superhard carbon allotrope. Its light weight virtue may make it as an ideal material for aerospace applications.

4. Conclusions

In summary, based on the bottom-up approach, we have proposed a new carbon allotrope, T-C_{56}, which can be considered as the assembled 3D solid from the stable cage isomer of C_{16} cluster with three types of cluster-cluster links. From our first-principles calculations, the following interesting features of T-C_{56} have been characterized: (i) it is a low-density (2.72 g cm^{-3}) porous material due to the existence of three

kinds of carbon hollow cages C_{16} [$4^2 5^8$], C_{20} [$4^4 5^4 6^4$] and C_{40} [$4^2 5^8 6^{12}$]; (ii) owing to the strong quasi-sp^3 bonds, it holds satisfied energy, dynamic and mechanical stabilities, and can even be more stable than the experimentally synthesized C20-sc and T-carbon; (iii) the analysis of electronic properties show that it is a transparent indirect wide bandgap (3.18 eV from HSE06) semiconductor without light adsorption in the visible region; (iv) the mechanical properties analysis reveals that it is a superhard material with considerable anisotropy. These results not only highlight a novel low-density superhard carbon allotrope, but also provide a new paradigm for the design of the desirable materials based on the cluster-assembled approach.

Acknowledgments

This work is supported by the National Natural Science Foundation of China (11964023 and 11604165) and Natural Science Foundation of Inner Mongolia (2016BS0104). The Cloud Computing Center of Lvliang 'Tianhe-2' is acknowledged for providing computational resources.

Notes

The authors declare no competing financial interest.

ORCID iDs

Xin Cui https://orcid.org/0000-0002-6858-4482
Zhifeng Liu https://orcid.org/0000-0002-8151-6839

References

[1] Kroto H W, Heath J R, O'Brien S C, Curl R F and Smalley R E 1985 *Nature* **318** 162
[2] Shvedova A, Castranova V, Kisin E, Schwegler-Berry D, Murray A, Gandelsman V, Maynard A and Baron P 2003 *J. Toxicol. Environ. Health* A **66** 1909
[3] Katsnelson M I 2007 *Mater. Today* **10** 20
[4] Mao H K and Hemley R J 1991 *Nature* **351** 721
[5] Mikitik G P and Sharlai Y V 2006 *Phys. Rev.* B **73** 235112
[6] Weng H, Liang Y, Xu Q, Yu R, Fang Z, Dai X and Kawazoe Y 2015 *Phys. Rev.* B **92** 045108
[7] Chen Y, Xie Y, Yang S A, Pan H, Zhang F, Cohen M L and Zhang S 2015 *Nano Lett.* **15** 6974
[8] Cui H-J, Yan Q-B, Sheng X-L, Wang D-L, Zheng Q-R and Su G 2017 *Carbon* **120** 89
[9] He C, Shi X, Clark S J, Li J, Pickard C J, Ouyang T, Zhang C, Tang C and Zhong J 2018 *Phys. Rev. Lett.* **121** 175701
[10] Wang J Q, Zhao C X, Niu C Y, Sun Q and Jia Y 2016 *J. Phys.: Condens. Matter* **28** 475402
[11] He C, Sun L, Zhang C, Peng X, Zhang K and Zhong J 2012 *Solid State Commun.* **152** 1560
[12] He C and Zhong J 2014 *Solid State Commun.* **181** 24
[13] He C, Sun L, Zhang C, Peng X, Zhang K and Zhong J 2012 *Phys. Chem. Chem. Phys.* **14** 8410
[14] He C, Zhang C X, Xiao H, Meng L and Zhong J X 2017 *Carbon* **112** 91
[15] Shi X, He C, Pickard C J, Tang C and Zhong J 2018 *Phys. Rev.* B **97** 014104
[16] Li Q, Ma Y, Oganov A R, Wang H, Wang H, Xu Y, Cui T, Mao H K and Zou G 2009 *Phys. Rev. Lett.* **102** 175506
[17] Wang J T, Chen C and Kawazoe Y 2011 *Phys. Rev. Lett.* **106** 075501
[18] Zhao Z, Xu B, Zhou X F, Wang L M, Wen B, He J, Liu Z, Wang H T and Tian Y 2011 *Phys. Rev. Lett.* **107** 215502
[19] Amsler M *et al* 2012 *Phys. Rev. Lett.* **108** 065501
[20] Umemoto K, Wentzcovitch R M, Saito S and Miyake T 2010 *Phys. Rev. Lett.* **104** 125504
[21] Yang X, Yao M, Wu X, Liu S, Chen S, Yang K, Liu R, Cui T, Sundqvist B and Liu B 2017 *Phys. Rev. Lett.* **118** 245701
[22] Zhang J *et al* 2017 *Nat. Commun.* **8** 683
[23] Wang Y, Panzik J E, Kiefer B and Lee K K M 2012 *Sci. Rep.* **2** 520
[24] Cui W, Yao M, Liu S, Ma F, Li Q, Liu R, Liu B, Zou B, Cui T and Liu B 2014 *Adv. Mater.* **26** 7257
[25] Sheng X L, Yan Q B, Ye F, Zheng Q R and Su G 2011 *Phys. Rev. Lett.* **106** 155703
[26] Wang J T, Nie S, Weng H, Kawazoe Y and Chen C 2018 *Phys. Rev. Lett.* **120** 026402
[27] Wang J T, Weng H, Nie S, Fang Z, Kawazoe Y and Chen C 2016 *Phys. Rev. Lett.* **116** 195501
[28] Jo J Y and Kim B G 2012 *Phys. Rev.* B **86** 075151
[29] Cote M, Grossman J C, Cohen M L and Louie S G 1998 *Phys. Rev.* B **58** 664
[30] Pickard C J and Needs R J 2010 *Phys. Rev.* B **81** 014106
[31] Zhou X F, Qian G R, Dong X, Zhang L X, Tian Y J and Wang H T 2010 *Phys. Rev.* B **82** 134126
[32] Jin Y J, Chen Z J, Xia B W, Zhao Y J, Wang R and Xu H 2018 *Phys. Rev.* B **98** 220103
[33] Li Z-Z, Wang J-T, Mizuseki H and Chen C 2018 *Phys. Rev.* B **98** 094107
[34] Rignanese G M and Charlier J C 2008 *Phys. Rev.* B **78** 125415
[35] Tans S J, Verschueren A R M and Dekker C 1998 *Nature* **393** 49
[36] McEuen P L 1998 *Nature* **393** 15
[37] Nistor R A, Newns D M and Martyna G J 2011 *ACS Nano* **5** 3096
[38] Liu J, Zhao T, Zhang S and Wang Q 2017 *Nano Energy* **38** 263
[39] Bu H, Zhao M, Dong W, Lu S and Wang X 2014 *J. Mater. Chem.* C **2** 2751
[40] Wei Q, Zhang Q, Yan H and Zhang M 2017 *J. Mater. Sci.* **52** 2385
[41] Omata Y, Yamagami Y, Tadano K, Miyake T and Saito S 2005 *Physica* E **29** 454
[42] Krätschmer W, Lamb L D, Fostiropoulos K and Huffman D R 1990 *Nature* **347** 354
[43] Iwasa Y *et al* 1994 *Science* **264** 1570
[44] Blase X, Gillet P, Miguel A S and Melinon P 2004 *Phys. Rev. Lett.* **92** 215505
[45] Yamanaka S, Kubo A, Inumaru K, Komaguchi K, Kini N S, Inoue T and Irifune T 2006 *Phys. Rev. Lett.* **96** 076602
[46] Wang J-T, Chen C-f, Wang D-S, Mizuseki H and Kawazoe Y 2010 *J. Appl. Phys.* **107** 063507
[47] Hu M, Tian F, Zhao Z, Huang Q, Xu B, Wang L-M, Wang H-T, Tian Y and He J 2012 *J. Phys. Chem.* C **116** 24233
[48] Soldatov A V, Roth G, Dzyabchenko A, Johnels D, Lebedkin S, Meingast C, Sundqvist B, Haluska M and Kuzmany H 2001 *Science* **296** 680
[49] Piskoti C, Yarger J and Zettl A 1998 *Nature* **393** 771
[50] Li D *et al* 2015 *J. Mater. Chem.* A **3** 10448
[51] Li Z, Hu M, Ma M, Gao Y, Xu B, He J, Yu D, Tian Y and Zhao Z 2016 *Carbon* **105** 151
[52] Jones R O and Seifert G 1997 *Phys. Rev. Lett.* **79** 443
[53] Qin J, He D, Wang J, Fang L, Lei L, Li Y, Hu J, Kou Z and Bi Y 2008 *Adv. Mater.* **20** 4780

[54] Kresse G and Furthmüller J 1996 *Phys. Rev.* B **54** 11169
[55] Perdew J P, Burke K and Ernzerhof M 1996 *Phys. Rev. Lett.* **77** 3865
[56] Hill R 1952 *Proc. Phys. Soc.* A **65** 349
[57] Chen X-Q, Niu H, Li D and Li Y 2011 *Intermetallics* **19** 1275
[58] Togo A, Oba F and Tanaka I 2008 *Phys. Rev.* B **78** 134106
[59] Petrescu M I 2004 *Diam. Relat. Mater.* **13** 1848
[60] Occelli F, Loubeyre P and LeToullec R 2003 *Nat. Mater.* **2** 151
[61] Birch F 1947 *Phys. Rev.* **71** 809
[62] Fan C-Z, Zeng S-Y, Li L-X, Zhan Z-J, Liu R-P, Wang W-K, Zhang P and Yao Y-G 2006 *Phys. Rev.* B **74** 125118
[63] Grimsditch M, Zouboulis E S and Polian A 1994 *J. Appl. Phys.* **76** 832
[64] Chen X-Q, Niu H, Franchini C, Li D and Li Y 2011 *Phys. Rev.* B **84** 121405
[65] Wu Z-J, Zhao E-J, Xiang H-P, Hao X-F, Liu X-J and Meng J 2007 *Phys. Rev.* B **76** 054115
[66] Le Page Y and Saxe P 2002 *Phys. Rev.* B **65** 104104
[67] Heyd J, Scuseria G E and Ernzerhof M 2003 *J. Chem. Phys.* **118** 8207
[68] Pugh S F 1954 *Phil. Mag.* **45** 823
[69] Frantsevich I N, Voronov F F and Bokuta S A 1983 *Elastic Constants and Elastic Moduli of Metals and Insulators* (Kiev: Naukova Dumka)
[70] Nye J F 1985 *Physical Properties of Crystals: Their Representation by Tensors and Matrices* (Oxford: Oxford University Press)
[71] Gao F, He J, Wu E, Liu S, Yu D, Li D, Zhang S and Tian Y 2003 *Phys. Rev. Lett.* **91** 015502
[72] Bu H, Zhao M, Wang A and Wang X 2013 *Carbon* **65** 341
[73] Wu X, Shi X, Yao M, Liu S, Yang X, Zhu L, Cui T and Liu B 2017 *Carbon* **123** 311
[74] Zhang S, Legut D, Fu Z, Germann T C and Zhang R 2018 *Carbon* **137** 156